Catalysts **2015**, *5*, 1275-1288; doi:10.3390/catal5031275

OPEN ACCESS

catalysts

ISSN 2073-4344

www.mdpi.com/journal/catalysts

Article

Facile Electrodeposition of Flower-Like PMo_{12}-Pt/rGO Composite with Enhanced Electrocatalytic Activity towards Methanol Oxidation

Xiaoying Wang, Xiaofeng Zhang, Xiaolei He, Ai Ma, Lijuan Le and Shen Lin *

College of Chemistry & Chemical Engineering, Fujian Normal University, Fuzhou 350007, China; E-Mails: cxwxy506@163.com (X.W.); xfz_fz@163.com (X.Z.); hexiaolei851@sina.com (X.H.); wyyd_1206@sina.com (A.M.); juanlile@163.com (L.L.)

* Author to whom correspondence should be addressed; E-Mail: shenlin@fjnu.edu.cn; Tel./Fax: +86-591-2286-7399.

Academic Editor: Minhua Shao

Received: 15 May 2015 / Accepted: 8 July 2015 / Published: 17 July 2015

Abstract: A facile, rapid and green method based on potentiostatic electrodeposition is developed to synthesize a novel $H_3PMo_{12}O_{40}$-Pt/reduced graphene oxide (denoted as PMo_{12}-Pt/rGO) composite. The as-prepared PMo_{12}-Pt/rGO is characterized by X-ray diffraction (XRD), scanning electron microscopy (SEM) and X-ray photoelectron spectroscopy (XPS). The results reveal that graphene oxide (GO) is reduced to the rGO by electrochemical method and POMs clusters are successfully located on the rGO as the modifier. Furthermore, the PMo_{12}-Pt/rGO composite shows higher electrocatalytic activity, better tolerance towards CO and better stability than the conventional pure Pt catalyst.

Keywords: reduced graphene oxide; phosphomolybdic acid; electrodeposition; methanol electrocatalytic oxidation

1. Introduction

Direct methanol fuel cells (DMFCs) have drawn increasing attention due to their simple operation, high energy density, low pollutant emission, low operating temperature (60–100 °C) and ease of handling liquid fuel [1–3]. It is widely agreed that, as a single component catalyst, platinum shows

significant electrocatalytic activity for methanol oxidation at lower temperatures. However, there are two key problems inhibiting its utilization in DMFCs: (1) high cost of precious platinum and (2) pure Pt electrocatalysts are prone to deactivation/ poisoning by the reaction intermediates (mainly CO), which generate from incomplete oxidation of methanol and chemically adsorb onto the Pt surface and block the active sites [4].

In order to decrease the usage of pure Pt electrocatalysts, various nanostructured carbon materials have been used to effectively disperse metal nanoparticles. In particular, reduced graphene oxide (rGO) has been found as a promising candidate for catalyst support in DMFCs [5]. Reduced graphene oxide (rGO) is gradually attracting more scientific and technological research interests due to its unique mechanical and electronic properties and wide applications [6,7]. On the other hand, polyoxometalates (POMs) are early-row transition metal oxygen anionic clusters with a remarkable redox and photo-electrochemical properties [8]. It was demonstrated [9] that Keggin-type $PMo_{12}O_{40}^{3-}$ anions in an aqueous solution could effectively convert carbon monoxide to carbon dioxide over catalysts, as represented by following equation.

$$[CO(g) + H_2O + PMo_{12}O_{40}^{3-}(aq) \rightarrow CO_2(g) + 2H^+(aq) + PMo_{12}O_{40}^{5-}(aq)] \quad (1)$$

In order to enhance CO tolerance in methanol oxidation and improve the durability of the Pt electrocatalysts, our group have studied the effects of silicotungstic acid ($H_4SiW_{12}O_{40}$) on the electrocatalytic activity of Pt catalysts towards methanol oxidation, and found that silicotungstic acid can promote the further oxidation of intermediates such as CO and supplies enough active sites for methanol oxidation [10]. Moreover, $H_3PMo_{12}O_{40}$ can also enhance electrocatalysis of Pd toward formic acid electrooxidation. The addition of $H_3PMo_{12}O_{40}$ contributes to converting CO into CO_2, which reduces the poisoning effects of CO over Pd catalyst [11]. All of these positive studies provide evidence that POMs could enhance antipoisoning ability of Pt in the methanol electrooxidation process on fuel cell anodes.

Up to now, many electrochemical methods have been used to reduce graphene oxide (GO) into reduced graphene oxide (rGO), such as cyclic voltammograms [12], potentiostatic electro deposition methods [13] and differential pulse voltammetry (DPV) [14]. The experiment results reveal that the electrochemical approach is a relatively economic, fast and environmental friendly method to prepare graphene avoiding toxic and hazardous chemicals such as hydrazine or dimethylhydrazine in the reduction process [15].

In this study, we firstly report a facile, fast, scalable, economic and environmentally benign pathway to prepare PMo_{12}-Pt/rGO composites. The electrochemical prepared approach can be undertaken via two steps (Figure 1): the first step involves direct electrochemical reduction of GO in suspension onto the substrate. Then, PMo_{12}-Pt clusters on the substrate surface were also deposited by electrodeposition method *in situ*. As expected, the as-prepared PMo_{12}-Pt/rGO composite exhibits superior catalytic activity on the electrochemical catalysis of methanol and CO oxidation.

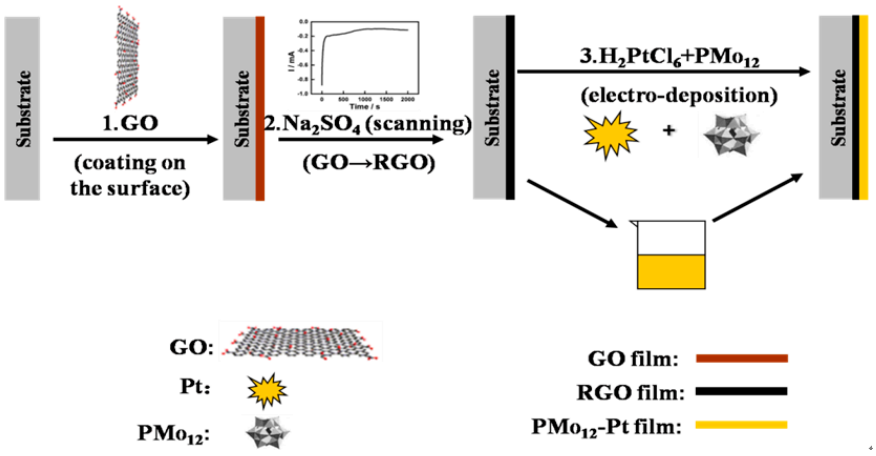

Figure 1. Schematic preparation of PMo_{12}-Pt/rGO composites.

2. Results and Discussion

Figure 2 displays the X-ray diffraction (XRD) patterns of rGO/indium tin oxide (rGO/ITO), Pt/rGO/ITO and PMo_{12}-Pt/rGO/ITO, respectively. As shown in Figure 2a, the diffraction peaks located at 30.23°, 35.16°, 50.47° and 60.02° can be considered as (222), (400), (440) and (622) crystal planes of ITO [16]. According to the ICDD PDF 04-0802, the diffraction peaks at 40.00°, 46.54°, 67.91° and 81.48° can be indexed to the (111), (200), (220) and (311) planes for Pt. These diffraction peaks are found in Figure 2b,c, which suggest that the successful formation of Pt on the rGO film by electrodeposition *in situ*. However, the diffraction peaks of Pt crystal planes (curve c) slightly shift comparing with curve (b). It may be as a result of the interaction among rGO, PMo_{12} and Pt. There are no distinct diffraction peaks of PMo_{12}, which may be due to the characteristic diffraction pattern of crystalline PMo_{12} being absent, which further implies that PMo_{12} clusters do not exist in the crystalline state but in the dispersed state [17].

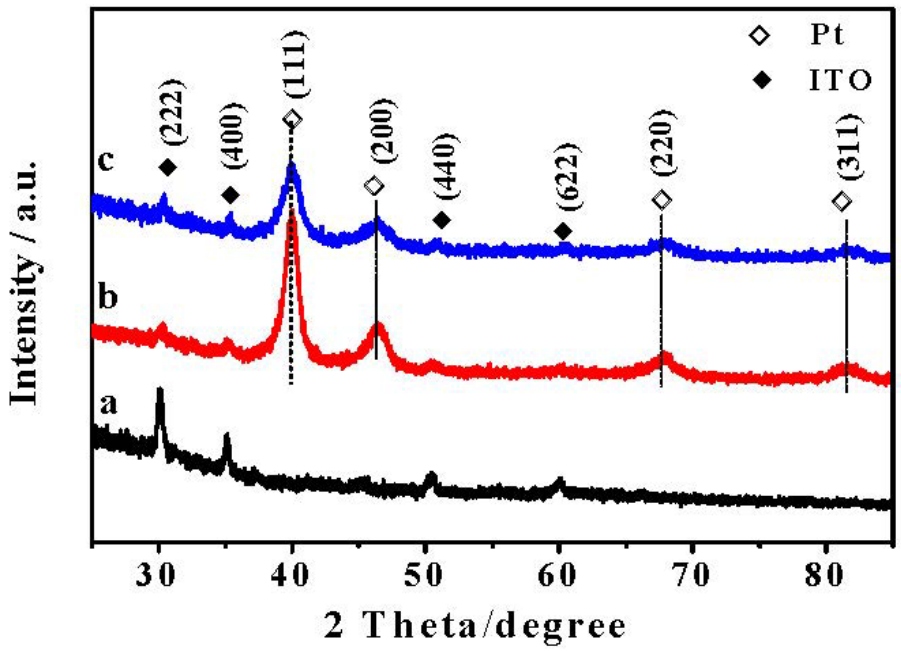

Figure 2. XRD patterns of the (**a**) rGO/ITO, (**b**) Pt/rGO/ITO and (**c**) PMo_{12}-Pt/rGO/ITO.

The presence of Pt, P, Mo, C, N, and O elements on the surface of the composite is confirmed in the full-spectra of X-ray photoelectron spectroscopy (XPS) (Figure 3a). As shown in Figure 3b, the C1s XPS spectrum of the prepared composite show that there are four kinds of carbon atoms in different functional groups: C–C/C=C bonds (284.6 eV), C–O bands (286.7 eV), C=O bands (287.5 eV) and O–C=O bands (288.5 eV) [18,19]. The C1s spectrum of GO shows the presence of two typical carbon bonds: C–C/C=C (284.6 eV) and C–O (286.7 eV) (Figure 3e). After electrochemical reduction, only the C–C/C=C bands remain dominant, which implies that the functional groups such as carboxyl groups, hydroxyl groups, and epoxy groups are reduced and detached from graphene surface. In Pt (4f) XPS of the composite (Figure 3c), the principle peaks are attributed to Pt° at 71.2 eV ($4f_{7/2}$) and 74.6 eV ($4f_{5/2}$) [20], while peaks at 72.1, 75.9 and 74.4, 77.5 eV are assigned to Pt in +2 and +4 states [21,22], respectively. The results of different Pt species are calculated based on above data and listed in Table S1. After electrolytic deposition by cyclic voltammetry, the relative intensity of Pt°, Pt^{2+} and Pt^{4+} are calculated to be 62.92%, 26.57% and 10.51% for prepared composite, respectively. However, in contrast, the proportion of Pt° on the surface is only 36.3% via chemical synchronous reduction [23]. Thus, the preparation method we used can effectively improve the content of Pt°. Moreover, the Mo 3d core level spectrum displays two peaks at binding energies of 232.8 eV and 236.0 eV, corresponding to the Mo $3d_{3/2}$ and Mo $3d_{5/2}$ spin-orbit states of PMo_{12}, respectively (Figure 3d) [24], which indicated the presence of PMo_{12} in the composite.

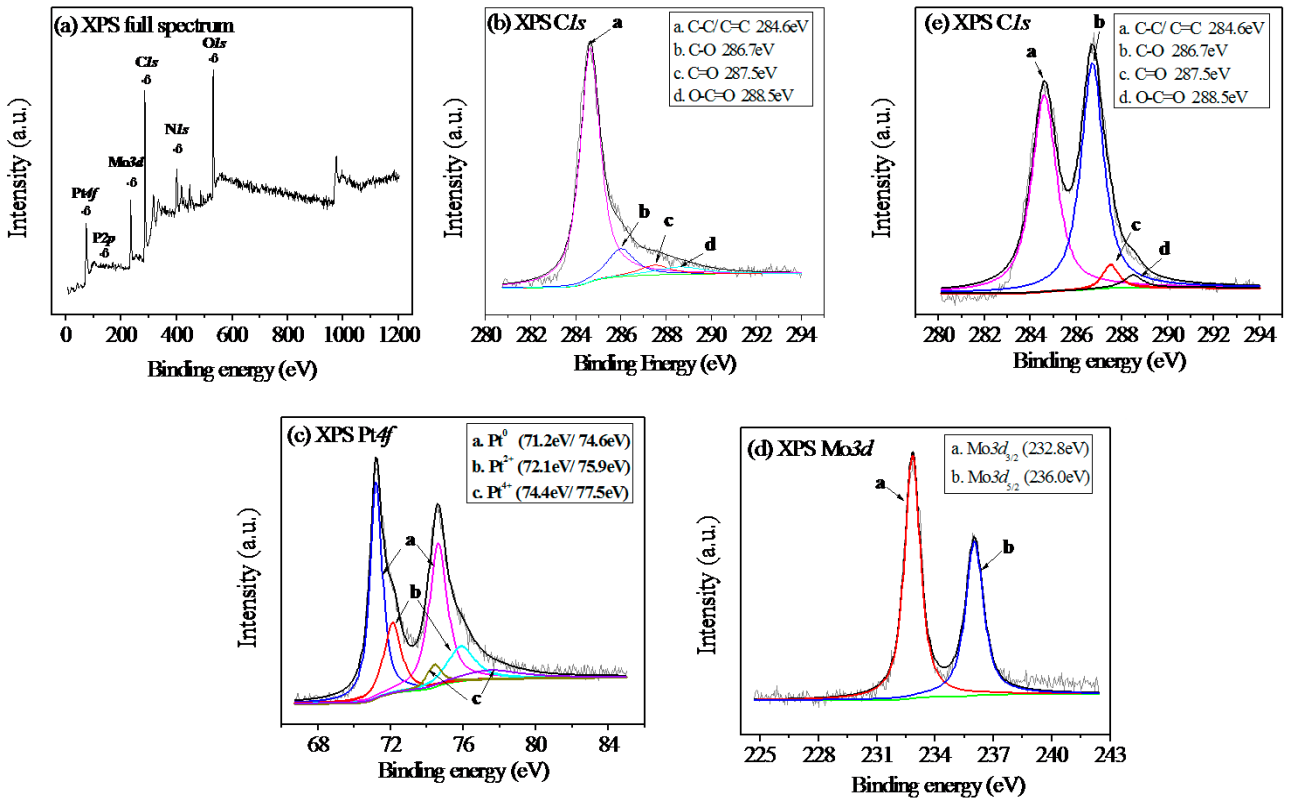

Figure 3. XPS spectra: (**a**) Full scan of PMo_{12}-Pt/rGO composites; (**b**) (**e**) C1s spectrum of PMo_{12}-Pt/rGO composites and GO; (**c**) (**d**) Pt 4f and Mo 3d spectrum of PMo_{12}-Pt/rGO composites.

Raman spectroscopy is a powerful nondestructive technique that is widely used to distinguish order and disorder in the crystal structure of carbon [25]. Figure 4 presents the Raman spectra of GO and PMo_{12}-Pt/rGO, respectively. Two groups of typical characteristic peaks of D bands and G bands can be observed at about ~1320 and ~1590 cm^{-1}, respectively. The D band originates from the disordered structural defects or edge areas, and the G band is associated with the in-plane vibration of sp^2 bonded carbon atoms [26]. Meanwhile, the intensity ratio of D and G bands (I_D/I_G) can be used to evaluate the extent of defects in carbonaceous materials. The I_D/I_G value of PMo_{12}-Pt/rGO is estimated about 1.80, which is higher than that of GO (1.33). The increase suggests the realization of deoxygenation during the reduction of GO [27].

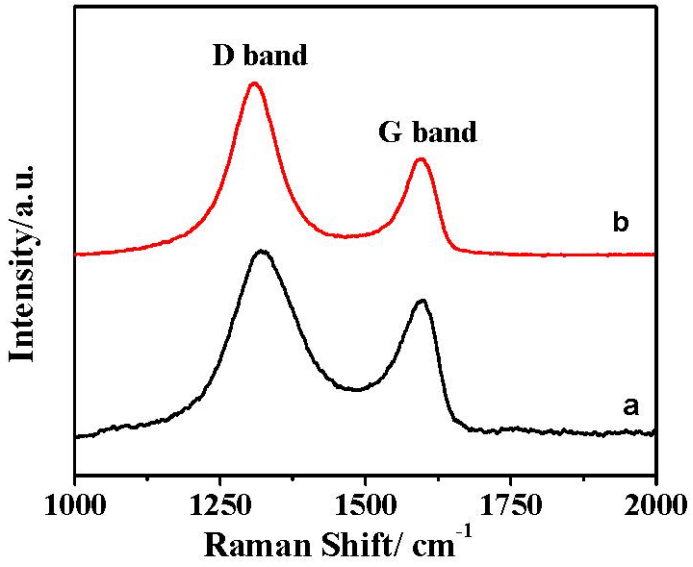

Figure 4. Raman spectra of different samples: (**a**) GO; (**b**) PMo_{12}-Pt/rGO.

Figure 5 displays the SEM images of different composites. Figure 5a–c are the surface morphology of PMo_{12}-Pt/ rGO/ITO composite, which are deposited at different electrode potentials. As shown in Figure 5a, when the deposition potential is −0.2 V, the coral-like clusters shape up on the rGO surface with the 100–800 nm diameters and less aggregation. When the deposition potential is −0.3 V, they are composed of flower-like clusters (Figure 5b) and the diameter is in range from 450 to 900 nm. Each flower-like cluster (Figure 5b inset) is three-dimensional, spear-shaped and multi-faceted. The mean diameter is of ~100 nm. These special structures may provide a larger specific surface area compared with other morphologies. When the deposition potential is decreased to −0.4 V, the PMo_{12}-Pt/rGO/ITO composite is in an irregular shape (Figure 5c).

Figure 5b,d and e presents the SEM images of PMo_{12}-Pt/rGO/ITO (b), Pt/rGO/ITO (d) and PMo_{12}-Pt/ITO (e) obtained from deposition potential of −0.3 V, respectively. As shown in Figure 5d, Pt clusters are spherical with diameters in the range of 100–450 nm and less aggregation. By contrast, PMo_{12}-Pt clusters are the same morphology as Pt/rGO with big size distribution (150–900 nm) in Figure 5e. It suggests that the introduction of the PMo_{12} and rGO may have an impact on the formation of the structure of clusters. Energy dispersive spectroscopy (EDS) analysis in Figure 5f identifies the presence of Pt, P, Mo, C, N and O on the PMo_{12}-Pt/rGO/ITO electrode and further confirms that PMo_{12}, Pt, and rGO are present in the composite.

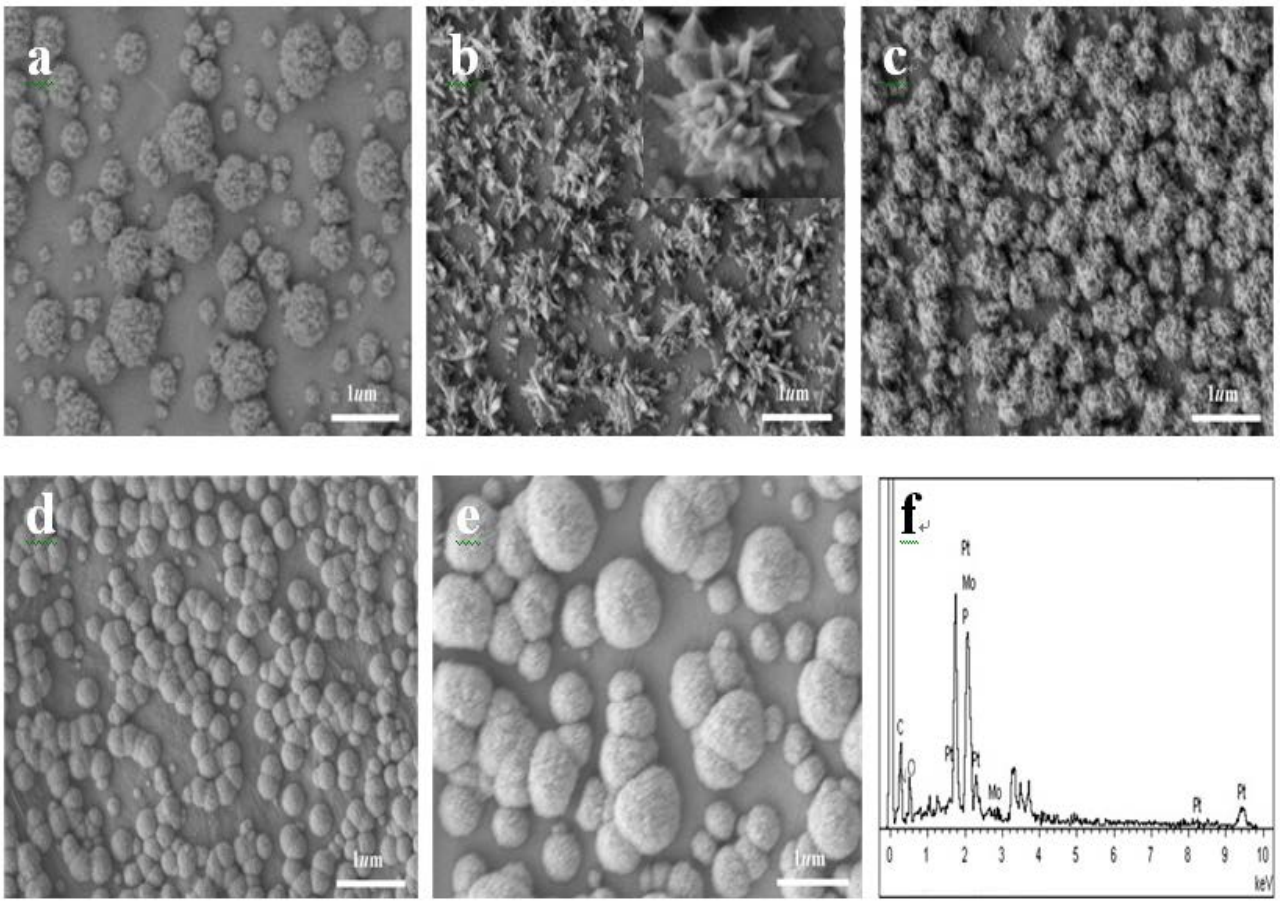

Figure 5. SEM images of different modified electrodes: (**a**) PMo_{12}-Pt/rGO/ITO composites at −0.2V; (**b**) PMo_{12}-Pt/rGO/ITO composites at −0.3V; (**c**) PMo_{12}-Pt/rGO/ITO composites at −0.4V; (**d**) Pt/rGO/ITO composites at −0.3V; (**e**) PMo_{12}-Pt/ITO composites at −0.3V. Scan time: 600 s; (**f**) EDS of PMo_{12}-Pt/rGO/ITO modified electrode at the deposition potential of −0.3V for 600 s.

The catalytic activity of the different modified electrodes was studied in a conventional three electrode system in 0.5 M H_2SO_4 + 1 M CH_3OH electrolyte solutions at a scan rate of 100 $mV \cdot s^{-1}$. Figure 6 presents the steady state cyclic voltammograms of Pt, Pt/rGO, PMo_{12}-Pt/rGO deposited on glassy carbon electrodes, referring to the Ag/AgCl electrode. The forward scan current density (I_f) of PMo_{12}-Pt/rGO/glass carbon electrode (PMo_{12}-Pt/rGO/GCE) was 269.1 $mA \cdot cm^{-2} \cdot mg^{-1}$ Pt, but it was 176.6 $mA \cdot cm^{-2}$ mg^{-1} Pt for Pt/rGO/GCE catalysts and only 147.9 $mA \cdot cm^{-2}$ mg^{-1} Pt for Pt/GCE catalysts. It is evident that the forward peak current value of PMo_{12}-Pt/rGO/GCE (about 269.1 $mA \cdot cm^{-2} \cdot mg^{-1}$ Pt) is 1.52 times higher than that of Pt/rGO/GCE (about 176.6 $mA \cdot cm^{-2}$ mg^{-1} Pt), which indicates that PMo_{12}-Pt clusters have better catalytic activity for methanol electrooxidation. The result may be explained as following: the poisonous intermediates such as CO that are absorbed on the active sites of Pt nanoparticles significantly can be catalytically oxidized by POMs, which results in the increased electrocatalytic activity of PMo_{12}-Pt clusters [28]. Therefore, PMo_{12}-Pt/rGO/GCE modified electrode for the oxidation of methanol in acidic medium shows better catalytic activity than Pt/rGO/GCE and Pt/GCE.

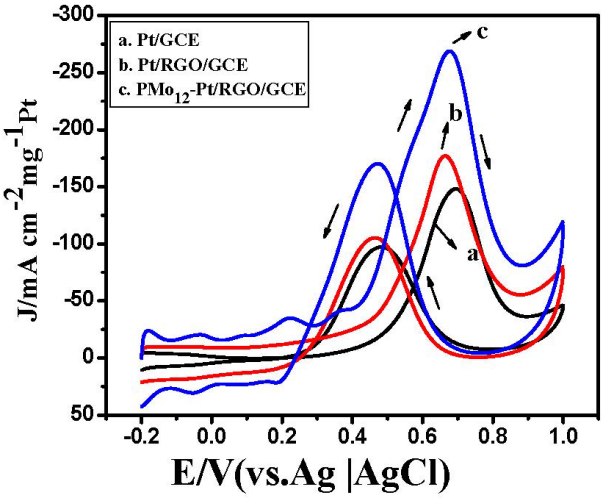

Figure 6. Cyclic voltammograms of different modified electrodes: (**a**) Pt/GCE; (**b**) Pt/rGO/GCE; (**c**) PMo_{12}-Pt/rGO/GCE in 0.5 M H_2SO_4 + 1 M CH_3OH solution. Scan rate: 100 $mV \cdot s^{-1}$.

The short-term stability of the catalysts was investigated by accelerated aging tests, which were performed by running the 1st time and 100 times between −0.20 V and 1.0 V with a scan rate of 0.10 $V \cdot s^{-1}$ in 0.5 M H_2SO_4 and 1 M CH_3OH aqueous solution for the catalysts are presented in Figure 7a–c. The peak for the Pt/GCE have the same change characteristics as that for the other electrodes with the increasing cycling number, but the electricity density for the Pt/GCE declines faster than the other electrodes (Figure 7a). However, for the Pt/rGO/GCE (Figure 7b) and PMo_{12}-Pt/rGO/GCE composite (Figure 7c), the current densities decline 11.33% and 6.99% (Table S2), respectively. Therefore, the PMo_{12}-Pt/rGO/GCE has better short-term stability than the other two.

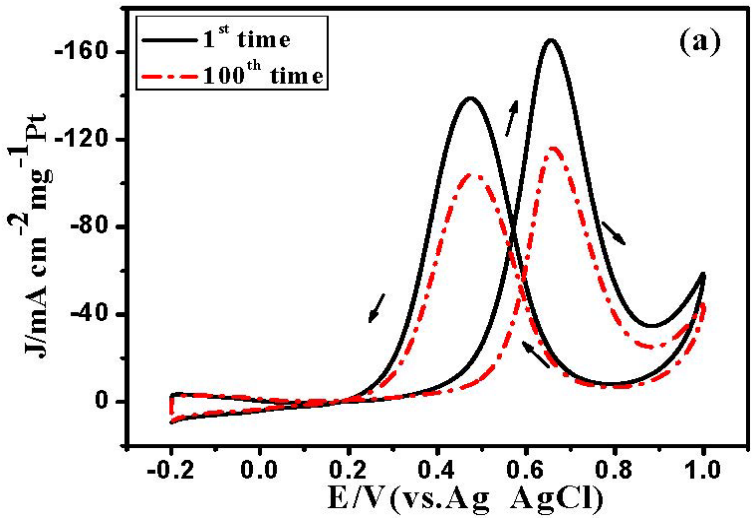

Figure 7. *Cont.*

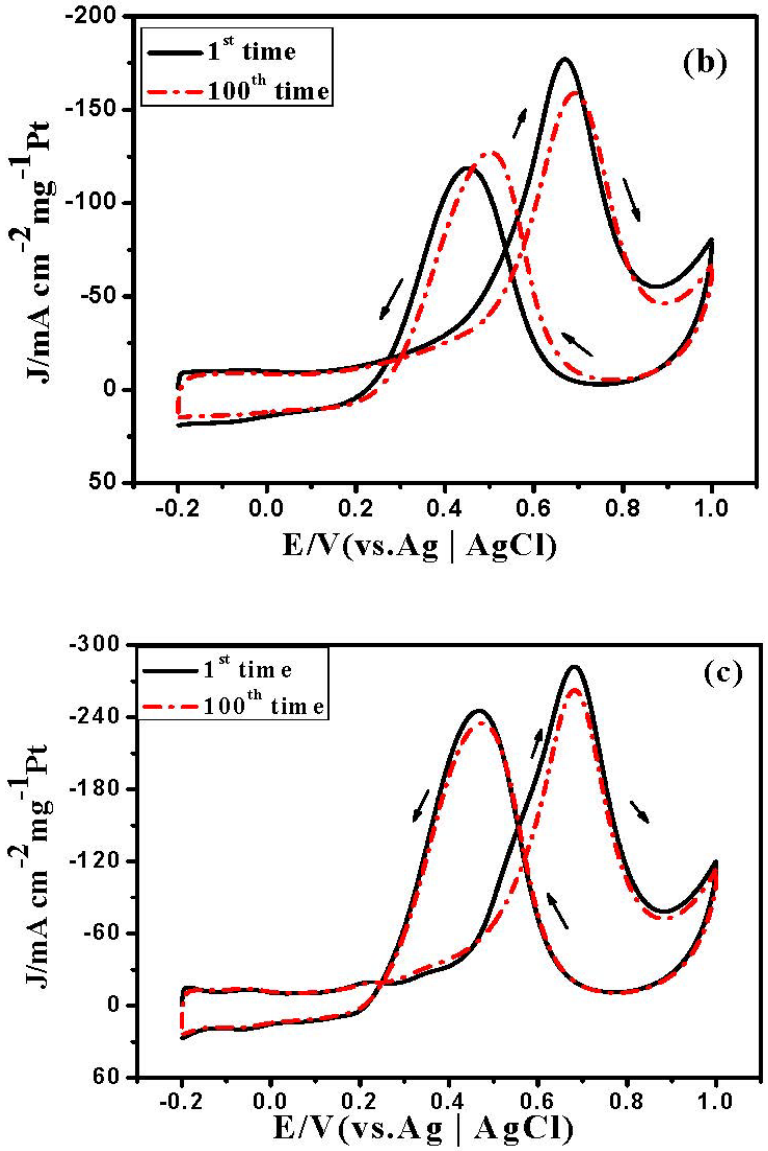

Figure 7. Comparative cyclic voltammograms of the different modified GCE electrodes: (**a**) Pt/GCE; (**b**) Pt/rGO/GCE; (**c**) PMo_{12}-Pt/rGO/GCE at 1st time and 100th times in 0.5 M H_2SO_4 + 1 M CH_3OH solution. Scan rate: 100 $mV \cdot s^{-1}$.

To evaluate the long-term performance of the three electrodes for methanol oxidation (in 0.5 M H_2SO_4 + 1 M CH_3OH solution), they were polarized at 0.68 V for 7200 s. As shown in Figure 8, a rapid initial current density decay is observed, due to the formation of some intermediate species (mainly CO_{ads}) during the methanol oxidation reaction [29]. Then the currents slowly decrease and reach a quasi-stationary state within 7200 s. As observed from Figure 9, the current densities at 7200 s are 6.18, 4.60, 2.81 $mA \cdot cm^{-2}mg^{-1} \cdot Pt$ towards methanol oxidation, respectively. The maximum steady-state oxidation current density for PMo_{12}-Pt/rGO/GCE is the largest compared to those of other electrodes. Thus, it confirms that the combination of PMo_{12}-Pt and rGO enhance electrocatalytic performance of the Pt catalyst.

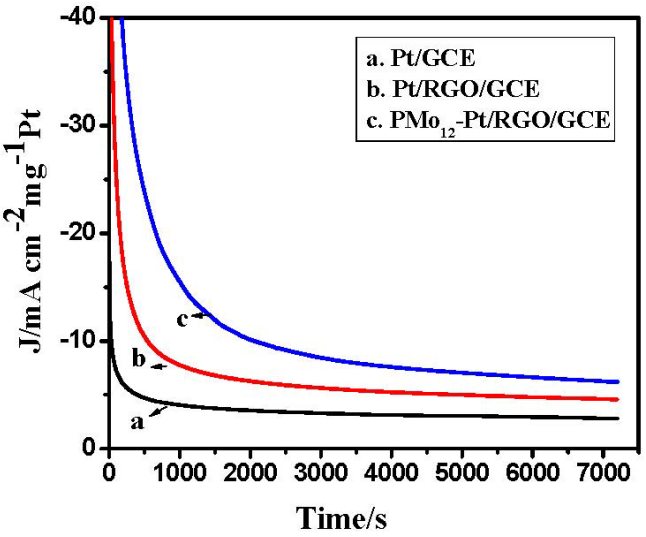

Figure 8. Chronoamperometric curves of different modified electrodes: (**a**) Pt/GCE; (**b**) Pt/rGO/GCE; (**c**) PMo_{12}-Pt/rGO/GCE in 0.5 M H_2SO_4 + 1 M CH_3OH solution at a fixed potential of 0.68 V for 2 h.

Electrochemical impedance spectroscopy (EIS) was used to further investigate the intrinsic behavior of the anodic process. The Nyquist plots of EIS for Pt/GCE (curve a), Pt/rGO/GCE (curve b), PMo_{12}-Pt/rGO/GCE (curve c) in 1 M CH_3OH + 0.5 M H_2SO_4 are shown in Figure 9. The diameter of the primary semicircle can be used to analyze the charge transfer resistance of the catalyst, and describe the rate of charge transfer during the methanol oxidation reaction [30]. The semicircle radius on the Nyquist plots of EIS for PMo_{12}-Pt/rGO/GCE is much smaller than that of Pt/GCE and Pt/rGO/GCE, clearly authenticating that the incorporation of PMo_{12} and rGO results in the improved conductivity of PMo_{12}-Pt/rGO/GCE.

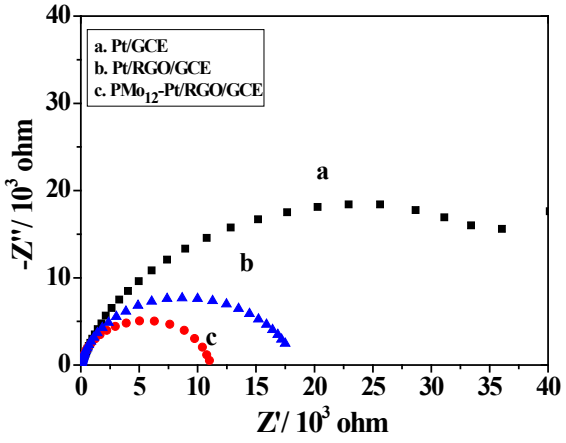

Figure 9. Nyquist plots of EIS with different films modified electrodes: (**a**) Pt/GCE; (**b**) Pt/rGO/GCE; (**c**) PMo_{12}-Pt/rGO/GCE in 0.5 M H_2SO_4 + 1 M CH_3OH solution.

Efficient elimination of the poisoning species such as CO from the catalyst is very important for assessing the catalyst performance in DMFCs. Figure 10 shows the voltammograms of CO oxidation on the different modified electrodes. As seen in Figure 10c, the distinct CO oxidation peak appears during the first forward scan, whereas it disappears in the second forward scan, indicating that

the adsorbed CO on the surface of PMo_{12}-Pt/rGO nanoparticles has been oxidized during the first forward scan [31]. The PMo_{12}-Pt/rGO/GCE exhibited the more negative peak potential (0.647 V), while the peak potential of Pt/rGO/GCE and Pt/GCE only 0.687 V and 0.729 V, respectively. The negatively shifted peak potentials indicate that CO species on the PMo_{12}-Pt/rGO interfaces are more easily transformed to CO_2 due to the oxidation ability of PMo_{12} [32]. Therefore, the active sites on Pt are released for further electrochemical reaction.

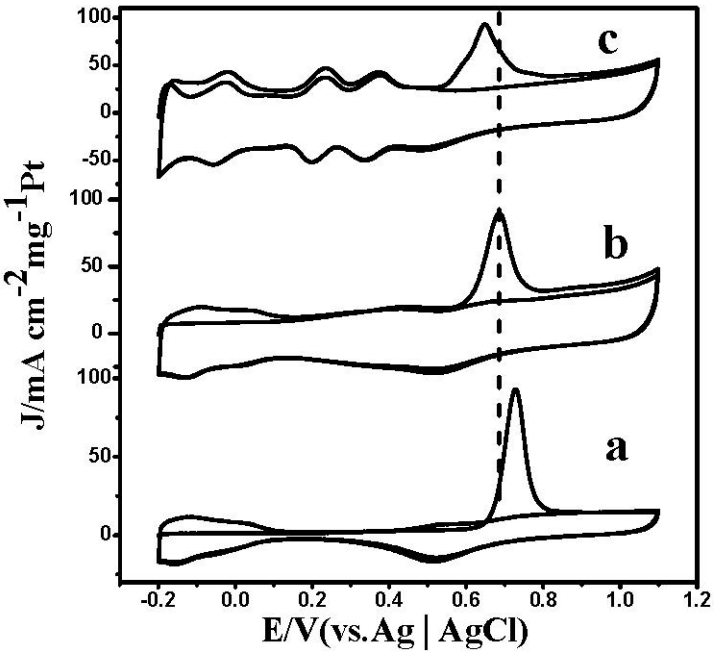

Figure 10. CO-stripping curves of different modified electrodes: (**a**) Pt/GCE; (**b**) Pt/rGO/GCE; (**c**) PMo_{12}-Pt/rGO/GCE in 0.5 M H_2SO_4 solution. Scan rate: 100 $mV \cdot s^{-1}$.

3. Experimental Section

3.1. Materials

Graphite powder (−325 mesh, 99.9995%) was purchased from Alfa Aesar (Shanghai, China). $Cu(Ac)_2$, K_2PtCl_4 (99%), $KMnO_4$, H_2O_2 (30%), $K_2S_2O_8$, P_2O_5, H_2SO_4, methanol, and ethanol were all purchased from Sinopharm Chemical Reagent Co., Ltd. (Shanghai, China) and used without further purification. Deionized water was used throughout the experiments.

3.2. Preparation of Reduced Graphene Oxide (rGO) Modified Electrode

Graphite oxide was prepared from graphite powder by a modified Hummers' method [33,34]. To obtain a homogeneous suspension, Graphite oxide was mixed with deionized water and ultrasonicated for 2 h. The as-prepared GO suspension was coated onto an indium tin oxide (ITO) glass or glass carbon electrode (GCE) to form GO film. The rGO film was prepared upon electrochemically reduction of GO film in 0.1 M Na_2SO_4 at a constant potential of −1.5 V for 600 s. (Figure 1).

3.3. Synthesis of PMo_{12}-Pt/rGO

PMo_{12}-Pt clusters were deposited *in situ* on the surface of the rGO film-modified GCE (3 mm in diameter) or ITO electrode (4 mm in width) by potentiostatic electrodeposition in a 0.5 M H_2SO_4 solution containing 2 mM H_2PtCl_6 and 0.2 mM PMo_{12} at −0.3 V for 600 s. After deposition, the working electrode was rinsed with distilled water and dried under an infrared lamp. For comparison, the electrodeposition of platinum on the surface of bare GCE or ITO, and rGO was also performed under the same conditions.

3.4. Characterization

XPS was performed at room temperature with monochromatic Al Kα radiation (1486.6 eV) using a Quantum 2000 system (PHI, Chanhassen, MN, USA). XRD patterns were measured on an X'pert Pro diffractometer (Philips, Almelo, The Netherlands), using Cu Kα radiation. Field emission scanning electron microscopy (FE-SEM) images were observed on a JSM-7500F field emission scanning electron microanalyzer (JEOL, Tokyo, Japan). EDS was used to confirm the existence of Pt particles. Ramam spectra was measured using a Renishaw-in-Via Raman (Renishaw, London, UK) micro-spectrometer equipped with 514 nm diode laser excitation on a 300 lines·mm^{-1} grating. The actual amount of Pt loadings of the catalysts was determined by inductively coupled plasma-mass spectroscopy (ICP-MS, X Series 2, Thermo Scientific, Waltham, MA, USA).

3.5. Electrochemical Measurements

Electrochemical measurements were conducted on a CHI660 Electrochemical Workstation (Chenhua, Shanghai, China) using a conventional three-electrode electrochemical system. The working electrode was a glassy carbon electrode (geometric area, 0.07 cm^2) modified with the catalysts; Ag/AgCl electrode and Pt wire were used as the counter and reference electrode, respectively. Cyclic voltammetric, EIS and chronoamperometric experiments were carried out in 0.5 M H_2SO_4 in the absence and presence of 1 M methanol. The electrolyte solution was deaerated with ultrahigh-purity N_2 before scanning. The CO stripping voltammograms were measured by oxidation of preadsorbed CO (CO_{ad}) in the 0.5 M H_2SO_4 solution at a scan rate of 100 mV·s^{-1}. CO was bubbled for 30 min to allow the complete adsorption of CO onto the composites when the potential was kept at 0.1 V. Excess CO in the electrolyte was then purged out with N_2 for 15 min.

CO-stripping curves of Pt/GCE, Pt/rGO/GCE, and PMo_{12}-Pt/rGO/GCE in 0.5 M H_2SO_4 solution is collected to evaluate the electrochemical surface areas (ECSA). All the composites show characteristic CO oxidation peak in the first forward scan, suggesting the presence of electrochemically active Pt. The ECSA were calculated by the integrated charge (Q) in the CO oxidation region. According to the equation ECSA = Q/(420 μC·cm^{-2} × Pt loading), we have added the Pt load for each sample in Table S3.

4. Conclusions

In this work, a unique flower-like PMo_{12}-Pt/rGO composite has been successfully synthesized by the electrochemical reduction method and used as an electrocatalyst for methanol oxidation. Cyclic

voltammetry, chronoamperometry and CO stripping voltammetry were used to study electrocatalytic properties of PMo_{12}-Pt/rGO composite in acidic medium for methanol oxidation. The PMo_{12}-Pt/rGO composite modified electrode shows higher catalytic activity, better electrochemical stability and resistance to CO poisoning, which may be attributed to the synergistic effect of the special morphology of the composite, excellent conductivity of rGO and superior redox properties of PMo_{12}. These findings suggest that the PMo_{12}-Pt/rGO composite can be considered as a good electrocatalyst material for DMFCs.

Acknowledgments

This project was financially supported by the National Natural Science Foundation of China (No. 21171037), the Natural Science Foundation of Fujian Province (No. 2014J01033) and a key item of Education Department of Fujian Province (No. JA13085 and JB13009).

Author Contributions

Xiaoying Wang, Xiaolei He and Lijuan Le did the experiments, Xiaoying Wang wrote the first draft, Ai Ma and Xiaofeng Zhang took part in the discussion of experiments results and revision of paper, Shen Lin was responsible for the research work and paper revision.

Conflicts of Interest

The authors declare no conflict of interest.

References

1. Kumar, P.; Dutta, K.; Das, S.; Kundu, P.P. An overview of unsolved deficiencies of direct methanol fuel cell technology: Factors and parameters affecting its widespread use. *Int. J. Energy Res.* **2014**, *38*, 1367–1390.
2. Li, Z.S.; Ji, S.; Pollet, B.G.; Shen, P.K. Supported 3-D Pt nanostructures: The straightforward synthesis and enhanced electrochemical performance for methanol oxidation in an acidic medium. *J. Nanopart. Res.* **2013**, *15*, 1959.
3. Singh, R.N.; Awasthi, R.; Sharma, C.S. An Overview of Recent Development of Platinum-Based Cathode Materials for Direct Methanol Fuel Cells. *Int. J. Electrochem. Sci.* **2014**, *9*, 5607–5639.
4. Yuan, T.; Yang, J.; Wang, Y.; Ding, H.; Li, X.; Liu, L.; Yang, H. Anodic diffusion layer with graphene-carbon nanotubes composite material for passive direct methanol fuel cell. *Electrochim. Acta* **2014**, *147*, 265–270.
5. Huang, Y.Q.; Huang, H.L.; Gao, Q.Z.; Gan, C.F.; Liu, Y.G.; Fang, Y.P. Electroless synthesis of two-dimensional sandwich-like Pt/Mn_3O_4/reduced-graphene-oxide nanocomposites with enhanced electrochemical performance for methanol oxidation. *Electrochim. Acta* **2014**, *149*, 34–41.
6. Liu, J.Q.; Liu, Z.; Barrow, C.J.; Yang, W.R. Molecularly engineered graphene surfaces for sensing applications: A review. *Anal. Chim. Acta* **2015**, *859*, 1–19.
7. Wang, X.; Liu, B.; Lu, Q.P.; Qu, Q.S. Graphene-based materials: Fabrication and application for adsorption in analytical chemistry. *J. Chromatogr. A* **2014**, *1362*, 1–15.

8. Khadempir, S.; Ahmadpour, A.; Ashraf, N.; Bamoharram, F.F.; Mitchell, S.G.; de la Fuente, J.M. A polyoxometalate-assisted approach for synthesis of Pd nanoparticles on graphene nanosheets: Synergistic behaviour for enhanced electrocatalytic activity. *RSC Adv.* **2015**, *5*, 24319–24326.
9. Seo, M.H.; Choi, S.M.; Kim, H.J.; Kim, J.H.; Cho, B.K.; Kim, W.B. A polyoxometalate-deposited Pt/CNT electrocatalyst via chemical synthesis for methanol electrooxidation. *J. Power Sources* **2008**, *179*, 81–86.
10. Zhang, X.F.; Huang, Q.F.; Li, Z.S.; Ma, A.; He, X.L.; Lin, S. Effects of silicotungstic acid on the physical stability and electrocatalytic activity of platinum nanoparticles assembled on graphene. *Mater. Res. Bull.* **2014**, *60*, 57–63.
11. Ma, A.; Zhang, X.F.; Li, Z.S.; Wang, X.Y.; Ye, L.T.; Lin, S. Graphene and Polyoxometalate Synergistically Enhance Electro-Catalysis of Pd toward Formic Acid Electro-Oxidation. *J. Electrochem. Soc.* **2014**, *161*, F1224–F1230.
12. Shao, Y.Y.; Wang, J.; Engelhard, M.; Wang, C.M.; Lin, Y.H. Facile and controllable electrochemical reduction of graphene oxide and its applications. *J. Mater. Chem.* **2010**, *20*, 743–748.
13. Ping, J.F.; Wang, Y.X.; Fan, K.; Wu, J.; Ying, Y.B. Direct electrochemical reduction of graphene oxide on ionic liquid doped screen-printed electrode and its electrochemical biosensing application. *Biosens. Bioelectron.* **2011**, *28*, 204–209.
14. Guo, H.L.; Wang, X.F.; Qian, Q.Y.; Wang, F.B.; Xia, X.H. A Green Approach to the Synthesis of Graphene Nanosheets. *ACS Nano* **2009**, *3*, 2653–2659.
15. Wang, Z.J.; Wu, S.X.; Zhang, J.; Chen, P.; Yang, G.C.; Zhou, X.Z.; Zhang, Q.C.; Yan, Q.Y.; Zhang, H. Comparative studies on single-layer reduced graphene oxide films obtained by electrochemical reduction and hydrazine vapor reduction. *Nanoscale Res. Lett.* **2012**, *7*, 1–7.
16. Sun, Z.Y.; He, J.B.; Kumbhar, A.; Fang, J.Y. Nonaqueous Synthesis and Photoluminescence of ITO Nanoparticles. *Langmuir* **2010**, *26*, 4246–4250.
17. Wang, S.; Li, H.L.; Li, S.; Liu, F.; Wu, L.X. Electrochemical-Reduction-Assisted Assembly of a Polyoxometalate/Graphene Nanocomposite and Its Enhanced Lithium-Storage Performance. *Chem. Eur. J.* **2013**, *19*, 10895–10902.
18. Li, H.L.; Pang, S.P.; Wu, S.; Feng, X.L.; Müllen, K.; Bubeck, C. Layer-by-Layer Assembly and UV Photoreduction of Graphene Polyoxometalate Composite Films for Electronics. *J. Am. Chem. Soc.* **2011**, *133*, 9423–9429.
19. Liu, R.J.; Li, S.W.; Yu, X.L.; Zhang, G.J.; Zhang, S.J.; Yao, J.N.; Zhi, L.J. A general green strategy for fabricating metal nanoparticles/polyoxometalate/graphene tri-component nanohybrids: Enhanced electrocatalytic properties. *J. Mater. Chem.* **2012**, *22*, 3319–3322.
20. Han, D.M.; Guo, Z.P.; Zeng, R.; Kim, C.J.; Meng, Y.Z.; Liu, H.K. Multiwalled carbon nanotube-supported Pt/Sn and Pt/Sn/PMo_{12} electrocatalysts for methanol electro-oxidation. *Int. J. Hydrogen Energy* **2009**, *34*, 2426–2434.
21. Roth, C.; Goetz, M.; Fuess, H. Synthesis and characterization of carbon-supported Pt–Ru–WO_x catalysts by spectroscopic and diffraction methods. *J. Appl. Electrochem.* **2001**, *31*, 793–798.
22. Liu, Z.L.; Guo, B.; Hong, L.; Lim, T.H. Microwave heated polyol synthesis of carbon-supported PtSn nanoparticles for methanol electrooxidation. *Electrochem. Commun.* **2005**, *8*, 83–90.

23. Xin, Y.; Liu, J.G.; Zhou, Y.; Liu, W.; Gao, J.; Xie, Y.; Zou, Z. Preparation and characterization of Pt supported on graphene with enhanced electrocatalytic activity in fuel cell. *J. Power Sources* **2011**, *196*, 1012–1018.
24. Bhattacharyya, K.; Majeed, J.; Dey, K.K.; Ayyub, P.; Tyagi, A.K.; Bharadwaj, S.R. Effect of Mo-Incorporation in the TiO_2 Lattice: A Mechanistic Basis for Photocatalytic Dye Degradation. *J. Phys. Chem. C* **2014**, *118*, 15946–15962.
25. Ji, Z.Y.; Shen, X.P.; Zhu, G.X.; Chen, K.M.; Fu, G.H.; Tong, L. Enhanced electrocatalytic performance of Pt-based nanoparticles on reduced graphene oxide for methanol oxidation. *J. Electroanal. Chem.* **2012**, *682*, 95–100.
26. Ding, Y.H.; Zhang, P.; Zhuo, Q.; Ren, H.M.; Yang, Z.M.; Jiang, Y. A green approach to the synthesis of reduced graphene oxide nanosheets under UV irradiation. *Nanotechnology* **2011**, *22*, 215601–215605.
27. Wang, C.Q.; Jiang, F.X.; Yue, R.R.; Wang, H.W.; Du, Y.K. Enhanced photo-electrocatalytic performance of Pt/RGO/TiO_2 on carbon fiber towards methanol oxidation in alkaline media. *J. Solid State Electrochem.* **2014**, *18*, 515–522.
28. Kang, Z.H.; Wang, Y.B.; Wang, E.B.; Lian, S.Y.; Gao, L.; You, W.S.; Hu, C.W.; Xu, L. Polyoxometalates nanoparticles: Synthesis, characterization and carbon nanotube modification. *Solid State Commun.* **2004**, *29*, 559–564
29. Dios, M.; Salgueirino, V.; Perez-Lorenzo, M.; Correa-Duarte, M.A. Synthesis of Carbon Nanotube-Inorganic Hybrid Nanocomposites: An Instructional Experiment in Nanomaterials Chemistry. *J. Chem. Educ.* **2012**, *89*, 280–283.
30. Ye, L.T.; Li, Z.S.; Zhang, L.; Lei, F.L.; Lin, S. A green one-pot synthesis of Pt/TiO_2/Graphene composites and its electro-photo-synergistic catalytic properties for methanol oxidation. *J. Colloid Interface Sci.* **2014**, *433*, 156–162.
31. Kim, M.S.; Fang, B.Z.; Chaudhari, N.K.; Song, M.Y.; Bae, T.S.; Yu, J.S. A highly efficient synthesis approach of supported Pt-Ru catalyst for direct methanol fuel cell. *Electrochim. Acta* **2010**, *55*, 4543–4550.
32. Zhao, X.; Zhu, J.B.; Liang, L.; Liu, C.P.; Liao, J.H. Enhanced electroactivity of Pd nanocrystals supported on $H_3PMo_{12}O_{40}$/carbon for formic acid electrooxidation. *J. Power Sources* **2012**, *210*, 392–396.
33. Zeng, Q.; Cheng, J.S.; Tang, L.H.; Liu, X.F.; Liu, Y.Z.; Li, J.H.; Jiang, J.H. Self-Assembled Graphene-Enzyme Hierarchical Nanostructures for Electrochemical Biosensing. *Adv. Funct. Mater.* **2010**, *20*, 3366–3372.
34. Hummers, W.S., Jr.; Offeman, R.E. Preparation of graphitic oxide. *J. Am. Chem. Soc.* **1958**, *80*, 1339.

© 2015 by the authors; licensee MDPI, Basel, Switzerland. This article is an open access article distributed under the terms and conditions of the Creative Commons Attribution license (http://creativecommons.org/licenses/by/4.0/).